RSC Advances

PAPER

View Article Online
View Journal | View Issue

Cite this: *RSC Adv.*, 2024, **14**, 22642

Optimizing white light emission in Dy(III) complexes: impact of energy transfer from mono and bidentate ligands on luminescence†

Sofia Malik,[a] Komal Jakhar,‡*[a] Devender Singh,‡*[a] Anjli Hooda,[a] Sonia Redhu,[a] Swati Dalal,[a] Vandana Aggarwal,[a] Sumit Kumar,[b] Rajender Singh Malik[b] and Parvin Kumar[c]

Complexes of dysprosium(III) ions with 1,1,1,5,5,5-hexafluoro-2,4-pentanedione featuring various mono and bi-dentate neutral ligands have been prepared and thoroughly investigated. The synthesized complexes exhibit an octa-coordinated environment, achieved by stoichiometrically combining organic ligands and Dy(III) ions. This octa-coordination environment of Dy(III) ion was confirmed by FT-IR spectroscopy, thermogravimetry and elemental analysis. Near-white light (NWL) is emitted when complexes were exposed to UV radiation, indicating a significant flow of energy from the sensitizing moieties towards the Dy(III) ion. This NWL emission might have resulted due to a balance between the intensities corresponding to emission peaks at 480 nm (blue) and 575 nm (yellow) in **Dy1–Dy3**. Emission spectra recorded at different excitation wavelength were utilized to study the tunability of CIE color coordinates. In addition to their high thermal stability, the complexes display bipolar paramagnetic shifts in their NMR spectra. The $^4F_{9/2} \rightarrow {}^6H_{13/2}$ transition, contributing ~62% of the total emission, stands out as a promising candidate for laser amplification due to its dominance in the emission spectra. Additionally, NWL emission observed in a solid Dy(III) complex opens intriguing possibilities for its application in next-generation white-light emitting devices.

Received 27th May 2024
Accepted 11th July 2024

DOI: 10.1039/d4ra03897e

rsc.li/rsc-advances

1 Introduction

There has been a strong push towards the development and wide spread use of energy efficient SSL (solid state lighting) technologies and smart devices in response to increased global demand for energy. Solid-state white-light-emitting materials offer remarkable benefits, like energy conservation and extended lifespan, leading to their widespread adoption across various applications, ranging from large-panel displays to lasers.[1–4] It is important to note that SSL sources can be classified based on the material used in their fabrication. For instance, LEDs employ inorganic phosphors, while OLEDs make use of organic semiconductors. Furthermore, SSLs can be categorized based on the method by which they emit light, with LEDs utilizing UV excitation and OLEDs relying on electrical excitation.[5,6] Considerable interest surrounds the realm of white light emission (WLE) which can be obtained using two different approaches: dual color emitters [blue either with red (B/R) or with yellow (B/Y)] or simply employing three-colour emitters that mix primary colors (RGB).[7–9] To generate white light, a variety of methods are employed, including the incorporation of different dopants or multiple phase matrices. These matrices can be composed of various materials like nanomaterials, organic compounds, hybrid organic–inorganic substances, metal complexes or inorganic phosphors. These materials have unique properties for achieving white light emission and sometimes combining these different materials is necessary to reach the desired outcome.

Additionally, WLE from single molecules is also attainable, covering entire visible spectrum.[10–12] Such systems comprises of a single-phase-single-emitter which eases the manufacturing process, resulting in materials which are light weight and thin, making them particularly well-suited for use in optical devices.[13] WLE from single molecules can be generated by utilizing trivalent lanthanide (Ln) complexes. The fascinating aspect of lanthanide luminescence is that it relies on indirect excitation of lanthanide ions, unlike other conventional photo-excitation methods. This is on account of parity restricted behavior of their f–f transitions which results in low absorptivity (0.5–3 $dm^3\ mol^1\ cm^1$).[14,15] To overcome this limitation,

[a]*Department of Chemistry, Maharshi Dayanand University, Rohtak, 124001, Haryana, India. E-mail: devjakhar@gmail.com*

[b]*Department of Chemistry, DCR University of Science & Technology, Murthal, 131039 Haryana, India*

[c]*Department of Chemistry, Kurukshetra University Kurukshetra, 136119, Haryana, India*

† Electronic supplementary information (ESI) available. See DOI: https://doi.org/10.1039/d4ra03897e

‡ The authors contributed equally to this work.

researchers have turned to suitable sensitizers, which possess the unique ability to indirectly transfer energy to lanthanide ions and function as antennas.[16,17] They absorb incident light and sensitize metal ion by efficiently transferring this energy to their excited states. Subsequently, excited Ln(III) ion engages in radiative relaxations to the lower electronic states. Narrow peaks are obtained in the emission spectra of these complexes due to the well-shielded 4f electrons of the lanthanide ions, which result in sharp and well-defined electronic transitions that are relatively unaffected by the ligand field and surrounding environment.

However, it is essential to highlight that selection of chromophoric sensitizer should be done carefully so that it functions as antenna along with producing its own emission in blue region which is basic necessity to produce white light.[18–20] This dual functionality is crucial for the production of white light when it is coordinated with the yellow light-emitting Dy^{3+} ion. Frequently employed antenna ligands include β-diketones and aromatic carboxylic acids, among others.[21–23] Along with these ligands, various neutral ligands like triphenylphosphine oxide, indazole, bipyridine, pyrazine *etc.* are also utilized in ternary complexes. These ligands apart from sensitizing the central metal ion, forms a protective coordination sphere to keep the high vibration solvent molecules away from the complex.[24,25] In this article, one $[Dy(hfpd)_3(M_2)]$ and three $[Dy(hfpd)_3(L)]$ (hfpd: 1,1,1,5,5,5-hexafluoro-pentane-2,4-dione), M: tri-*n*-octylphosphineoxide (TOPO), L: 1,10-phenanthroline (phen), neocuproine (neoc) and bathocuproine (bathoc) type of complexes were synthesized. The ligands used in the synthesis have high probability to coordinate with Ln^{3+} ions due to the strong affinity of oxygen and nitrogen atoms towards lanthanide ions and their π–π* transitions result in strong UV absorption and efficiently sensitize Ln^{3+} ions. The $[Dy(hfaa)_3phen]$ complex[26] has been previously documented in the literature. The potential applications of these complexes span a broad spectrum, covering diverse fields such as solid-state lighting, chemical and biological sensing, temperature monitoring and telecommunication.[27–29]

2 Experimental section

2.1 Materials

$DyCl_3 \cdot 6H_2O$, hfpd, TOPO, phen, neoc and bathoc of high purity were sourced from Sigma Aldrich. AR or spectroscopic grade hexane and ethanol along with reagent 25% ammonia solution were sourced from Sigma-Aldrich. All the procured chemicals were employed as received and the reactions were performed under ambient conditions.

2.2 Method

Quantification of carbon, hydrogen and nitrogen contents was achieved by employing Series II PerkinElmer Elemental Analyser (2400). While, FT-IR spectra (4000–400 cm^{-1}) were collected employing a Nicolet iS-50 FTIR spectrometer. The KBr pellets were formed by incorporating a small quantity of the complex into KBr and then thoroughly grounding it. ^1H NMR spectra were recorded using a FT-NMR spectrometer in $CDCl_3$. Shimadzu 2450 UV-visible spectrophotometer was employed to observe electronic spectra ranging 200–800 nm. Photoluminescent (PL) properties were analyzed through Horiba Jobin YVON Fluorolog Model FL-3-11 spectrofluorometer equipped with xenon lamp as light source and 0.5 mm excitation and emission slit width. A Fluorescence Spectrophotometer was utilized to investigate the lifetimes of the prepared samples. The current–voltage relationship was characterized at a scan rate of 0.1 V s^{-1} using the PARSTAT 4000 instrument. The complexes were subjected to thermal analyses under a N_2 at temperature rise of 10 °C per minute, utilizing Hitachi STA thermal analyzer 7300 and the findings are presented in the form of a thermogram.

2.3 Synthesis of ternary Dy^{3+} complexes

Synthesis of dysprosium(III) complexes was carried out using an *in situ* approach (Fig. 1).[30,31] 25% NH_4OH solution was added to 5 mL ethanolic solution of 6.48 mmol hfpd. The contents were kept in a 50 mL container and sealed until the complete dissolution of ammonia vapours which led to the formation of ammonium salt of hexafluoroacetylacetone, $[NH_4(hfpd)]$. Subsequently, this mixture was combined with 5 mL solution of 2.16 mmol $DyCl_3 \cdot 6H_2O$ solution in ethanol and further ethanolic solution of neutral ligand was added. The stoichiometric relationship between $DyCl_3 \cdot 6H_2O$, hfpd and neutral ligands was 1 : 3 : 1 in **Dy2–Dy4** complex and 1 : 3 : 2 in **Dy1**. This mixture was kept within a pH range of 6–7 and underwent stirring for 12 h at room temperature. Completion of synthetic reaction was marked by formation of precipitates of **Dy1**, **Dy2**, **Dy3** and **Dy4** with TOPO, phen, neoc and bathoc, respectively. The mixtures were left for slow evaporation at room temperature and the formed precipitates underwent repeated washing with both ethanol and hexane.

3 Findings and interpretation

3.1 Preliminary assessment

CHN analysis was conducted for precise establishment of elemental composition of synthesized trivalent dysprosium compounds. The elemental analysis findings showed close approximation with calculated elemental content, indicating that the complexes were prepared in the correct stoichiometry. Moreover, all the compounds displayed solubility in dichloromethane, chloroform and dimethyl sulphoxide under standard laboratory conditions. Table 1 presents the color and elemental composition for **Dy1** to **Dy4**.

3.2 IR spectroscopy study

The application of IR spectroscopy enables the determination of bonding of ligand with emissive ion. hfpd chelates with Dy^{3+} ion were formed through a covalent bond with enolic oxygen(=C–O) and a coordinate bond with carbonyl oxygen (–C=O), resulting in stable complexes. Table 2 provides information of the peaks associated with the synthesized complexes. The unbound ligand (hfpd) exhibits a band ~3400 cm^{-1}, in relation

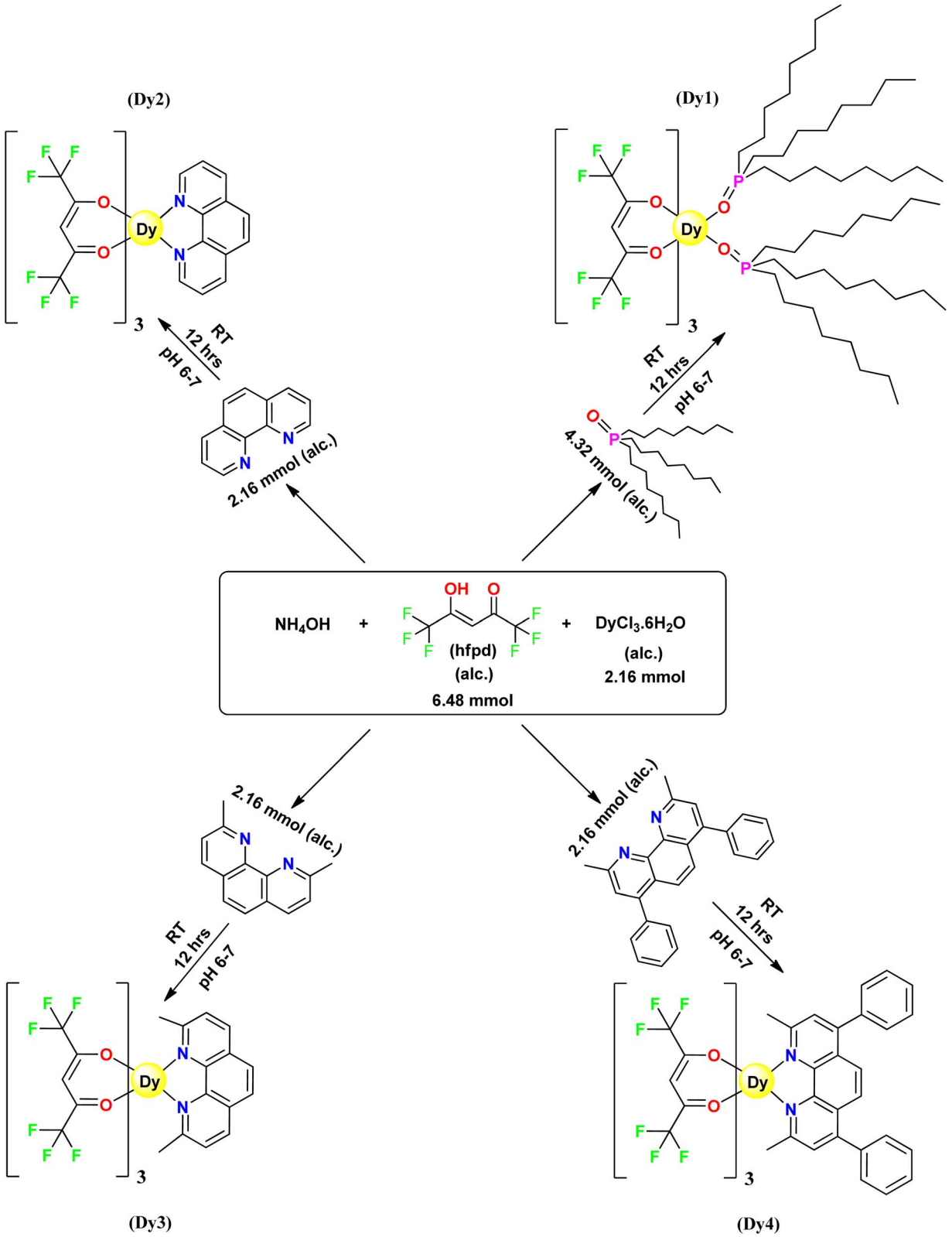

Fig. 1 Schematic pathway for preparation of Dy1–Dy4.

to =C–OH stretch. Absence of this stretching vibration band in complexes indicates the chelation of Dy(III) *via* deprotonated ligand in its enol form (C=C–O). Additionally, peaks around 1690 and 1636 cm^{-1} relative to carbonyl vibration of enol-isomer and C=C stretching, respectively in free hfpd[32] are displaced to 1660 cm^{-1} and 1434 cm^{-1} in **Dy1–Dy4**,

Table 1 Primary findings of C, H and N component in % of **Dy1–Dy4**

Complex	Colour shown	C calcd. (Expt.)	H calcd. (Expt.)	N calcd. (Expt.)
Dy1	White	48.60 (48.65)	6.80 (6.78)	—
Dy2	White	33.65 (33.61)	1.15 (1.18)	2.91 (2.93)
Dy3	Cream	35.12 (35.17)	1.52 (1.50)	2.82 (2.85)
Dy4	Light yellow	43.04 (43.09)	2.03 (2.01)	2.45 (2.49)

Table 2 Key findings from FT-IR spectroscopic analysis of **Dy1–Dy4** (cm^{-1})

Complex	Dy–O	Dy–N	C–H	C–F	P=O	C–N	C=C	C=N	C=O	CH_3	=C–H
Dy1	425	—	844	1146	1204	—	1427	—	1663	2858	3105
Dy2	428	554	842	1144	—	1349	1428	1556	1653	—	3058
Dy3	426	546	851	1146	—	1355	1434	1553	1651	2834	3062
Dy4	426	541	854	1154	—	1357	1441	1542	1662	2841	3055

highlighting the potential participation of C=O in coordination processes. Complexes exhibit multiple peaks corresponding to CF_3 groups in the range 1144–1154 cm^{-1}, which are observed in the range 1368–1090 cm^{-1} in free hfpd ligand.[33]

The free phen ligand displays the C–H bending vibration at 857 cm^{-1} as well as C=C and C=N ring vibrations in 1650–1400 cm^{-1} range.[34] Discussed peaks undergo significant downward shifts in wavenumber to 842 cm^{-1} in mononuclear [Dy(hfpd)$_3$phen] complex as a result of perturbation brought on by coordination of ligand to metal ion. Similarly, free TOPO exhibits a peak at 1210 cm^{-1} ascribed to P=O that is shifted towards 1204 cm^{-1} in **Dy1**.[35] Moreover, the complexes exhibit low-intensity peaks around 425–428 cm^{-1}, associated with Dy–O modes and at ~546 cm^{-1}, attributed to Dy–N coordination in **Dy2–Dy4** complexes.[36] Such changes in spectrum suggest that Dy(III) ion not only coordinates with carbonyl oxygen of hfpd but also directly interacts with two nitrogen atoms of phen and its derivatives in **Dy2–Dy4** and two oxygen atoms of TOPO in **Dy1** complex. The lack of vibrational band between 3600 and 3200 cm^{-1} indicates that water molecules are absent in **Dy1–Dy4**.[37]

3.3 ^{1}H NMR analysis

Proton NMR spectra of the synthesized complexes (Fig. S1–S4†) were recorded in $CDCl_3$ at a bandwidth of 500 MHz and the obtained chemical shifts are outlined in Table 3. Salient features of the spectra are as follows: (i) in comparison to uncoordinated ligands, the complexes exhibit significant upfield and downfield shifts[38] (ii) instead of the anticipated 4 peaks, complex **Dy2** displayed only 3 peaks corresponding to phen. Notably, one proton signal was absent within the range of +200 to −200 ppm, owing to the higher magnetic moment of dysprosium ion and resulting in paramagnetically enhanced relaxation of this nucleus (iii) opposite shift directions are observed for methine protons (hfpd) and ancillary ligand protons in **Dy1–Dy4** (iv) the absence of a signal relative to enolic OH of hfpd in the spectral profiles of complex implies the binding of the Dy^{3+} ion to the oxygen atom of hfpd.[26,39]

3.4 UV-vis absorption spectroscopy

Fig. 2 illustrates room temperature electronic spectra of free hfpd and **Dy1–Dy4**, captured in 1×10^{-5} mol L^{-1} dichloromethane solution. The uncoordinated hfpd displays a prominent absorption band at 279 nm, predominantly associated with spin-allowed $\pi \rightarrow \pi^*$ transitions. In contrast, the UV-vis absorption spectra of **Dy1–Dy4**, besides the UV absorption band at 243–277 nm, reveal a broad maxima at 287–314 nm owing to corresponding transitions of $\pi \rightarrow \pi^*$ and $n \rightarrow \pi^*$. The initial band in each spectrum (shorter-wavelength band), corresponds to the ancillary ligand.[40] Complexation leads to a red-shift in the absorption bands of β-diketone ligands, revealing stabilization of their orbitals (nephelauxetic effect).[41] Table 4 comprises of absorption maxima corresponding to **Dy1–Dy4**.

For **Dy1–Dy4** complexes, the determined molar absorption coefficients (ε) are 1.4×10^4, 2.91×10^4, 6.24×10^4, and $1.07 \times$

Table 3 Proton δ (ppm) data of **Dy1–Dy4**

Complex	Peaks relative to hfpd	Peaks relative to ancillary moiety
hfpd	10.85 (-OH), 6.48 (-C-H)	—
Dy1	101.47 (3H)	−1.48 (18H), −3.42 & −3.81 (60H), −5.89 (12H), −7.72 (12H)
Dy2	117.36 (3H)	−28.72 (2H), −42.64 (2H), −60.90 (2H)
Dy3	134.10 (3H)	−1.34 (6H), −32.85 (2H), −48.11 (2H), −62.86 (2H)
Dy4	128.08 (3H)	−2.19 (6H), −33.22 (2H), −48.18 (2H), −61.39 (10H)

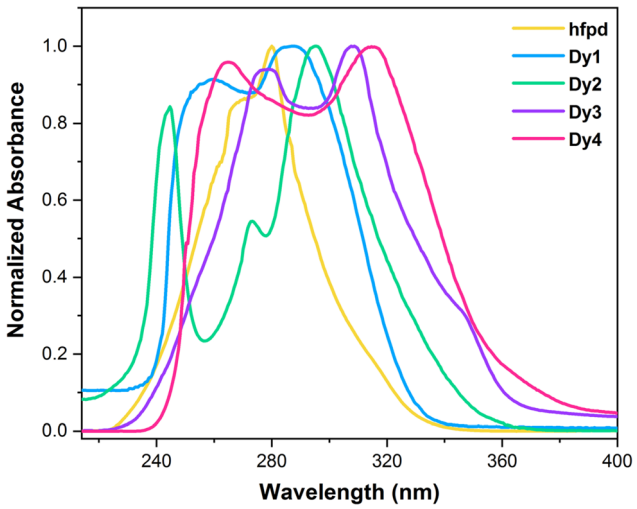

Fig. 2 Absorption spectra of free hfpd and **Dy1–Dy4** complexes.

Table 4 Optical parameters for **Dy1–Dy4**

Complex	$^{a}\lambda_{abs}^{max}$	$^{a}E_g$	$^{a}\lambda_{ex}$	$^{a}\lambda_{em}$
Dy1	286	3.87	279, 371	485, 575, 661
Dy2	295	3.79	278, 370	486, 574, 662
Dy3	308	3.70	279, 372	486, 574, 660
Dy4	314	3.55	302, 374	574, 662

^{a} λ and E in nm and eV, respectively.

10^5, respectively (Fig. S5†). Compared to the ε of free hfpd, which is 6.7×10^3,[42] these values are approximately threefold higher. This result shows that inclusion of ancillary ligands not only meets the coordination needs of the Dy(III) ion but also enhances the absorption intensity. The lowest ε value observed for complex **Dy1** can be attributed to the lack of an extended π-system, resulting in less efficient light absorption. In contrast, **Dy4** exhibits the highest ε value due to its more extended π-system, which significantly enhances its ability to absorb light. Band gap (E_g) of aforementioned compounds is also measured utilizing eqn (1) *i.e.* Tauc's equation, on data obtained from electronic spectra:[43]

$$(\alpha h\nu)^2 = A(h\nu - E_g)^n \quad (1)$$

Here, α denotes absorptivity, $h\nu$ denotes energy of photon, A is used to signify the band edge parameter, while E_g symbolizes the optical band gap. The parameter n is a transition-dependent factor with a value of 1/2 for indirect and 2 for direct excitation.[44] E_g values of **Dy1–Dy4** were measured by the help of Tauc plot between energy and $(\alpha h\nu)^2$ as shown in Fig. 3. This was accomplished by extrapolation of straight line to $(\alpha h\nu)^2 = 0$. E_g of **Dy1–Dy4** complexes in eV are detected as 3.87, 3.79, 3.70 and 3.55, respectively. This decreasing order in the band gap is attributed to the increasing conjugation in synthesized complexes. The effectiveness of the considered complexes in display devices is closely tied to E_g values falling in semiconductor range, contributing to enhanced performance in electronic technologies.[45]

3.5 Photoluminescence spectroscopy investigations

3.5.1 Excitation spectra. To analyze photoluminescent behaviour exhibited by **Dy1–Dy4**, solid samples were excited using emission wavelengths (λ_{em}) of 480 nm ($^4F_{9/2} \rightarrow {}^6H_{15/2}$) and 575 nm ($^4F_{9/2} \rightarrow {}^6H_{13/2}$). However, the spectra recorded at 575 nm was more intense in comparison to the one recorded at 480 nm. Normalized excitation spectrum ($\lambda_{em} = 575$ nm) (Fig. 4) of each complex revealed ligand based broad bands ~280 and ~370 nm (Table 4) relative to energy required for an electron to jump from π to π*.[46,47] Since, no metal centered peaks were observed in the excitation spectra and the spectral profiles are dominated by ligand's absorption, it suggests that sensitization in **Dy1–Dy4** happened *via* indirect energy transfer [ligand → Dy(III)]. The excitation spectra of **Dy1–Dy4** exhibit different intensities with **Dy3** being most intense and **Dy4** being least intense.

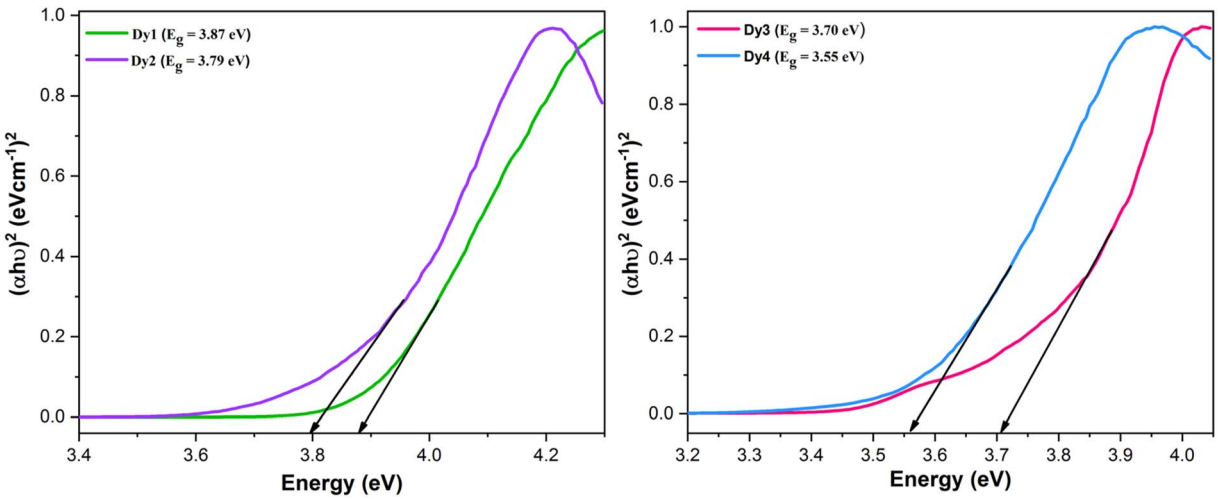

Fig. 3 Tauc's plots and band gap values of **Dy1–Dy4** complexes.

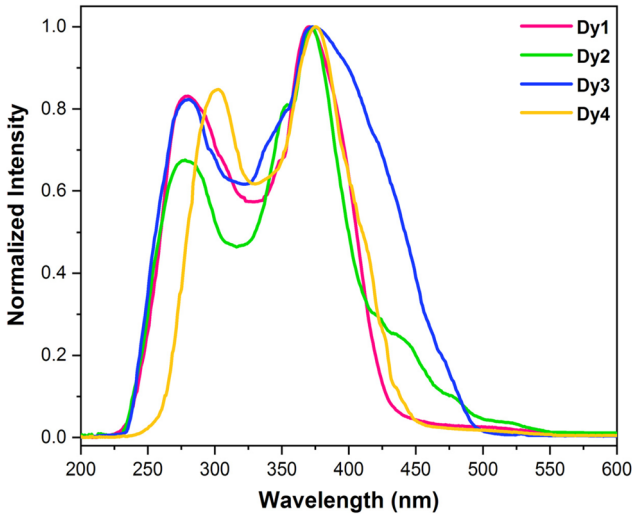

Fig. 4 Normalized excitation spectra of solid **Dy1–Dy4** at room temperature at λ_{em} = 575 nm.

3.5.2 Emission spectra. Fig. 5 contains the normalized emission profiles of solid **Dy1–Dy4** complexes. The spectral profiles exhibit emission peaks (Table 4) associated with $^4F_{9/2} \rightarrow {}^6H_{x/2}$ (x = 15, 13, 11) and π–π* transitions of organic moieties, upon excitation at ~370 nm. These peaks correspond to three different electronic transitions: a blue, magnetic-dipole (MD) transition ($^4F_{9/2} \rightarrow {}^6H_{15/2}$) at ~486 nm; a yellow, electric-dipole (ED) transition ($^4F_{9/2} \rightarrow {}^6H_{13/2}$) at ~574 nm and a least intense peak at ~661 nm.[48,49] The transition at ~574 nm is most intense and sensitive to its environment. The greater intensity of transition centered at 574 nm indicates that complexes are situated in low molecular symmetry and lack inversion centre. This makes the yellow transition a valuable reference for assessing symmetry in such systems. While magnetically allowed blue emission ($^4F_{9/2} \rightarrow {}^6H_{15/2}$) remains unaffected by the local environment surrounding Dy(III) ion.[50] A broad band at lower wavelength is exhibited by all the complexes due to transition from ligand's excited state to ground state indicating that the ligands do not transfer the absorbed energy effectively to the emissive state of metal ion which is discussed in detail in Section 3.5.7. Moreover, the emission spectrum of **Dy4** exhibits only 2 metal based peaks (at 574 nm and 662 nm) along with a broad ligand based band which merged with the third peak (485 nm).

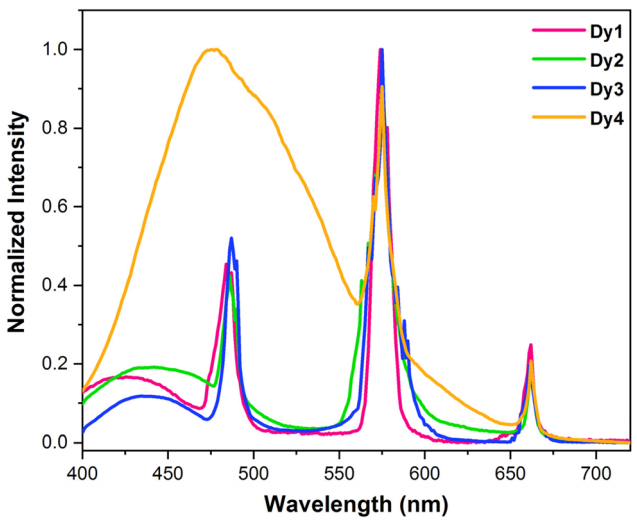

Fig. 5 Normalized emission spectra of solid **Dy1–Dy4** obtained at room temperature with λ_{ex} = ~370 nm.

3.5.3 Branching ratio. Calculating the branching ratio (β) involves the comparison between radiative transition probability for each peak and combined radiative transition probability of all peaks as expressed in eqn (2).[51]

$$\beta = \frac{A_{\psi J-\psi' J}}{\sum A_{\psi J-\psi' J}} \times 100 \quad (2)$$

Here, $A_{\psi J-\psi' J}$ denotes the total area under the observed peak in photoluminescence emission (PLE) spectrum of **Dy1–Dy4** compounds. The importance of β in laser design lies in its role in determining the chances of stimulated emission from particular emission transitions. A greater β value indicates a higher suitability for achieving stimulated emission cross-section.[52] Table 5 presents the calculated branching ratios for **Dy1–Dy4**. Analysis of β ratios reveals a predominance of $\Delta J = 2$ transition, accounting for ~60% of the total emission in **Dy1–Dy3**. This suggests its suitability for laser amplification.[53] The yellow emission originating from $\Delta J = 2$ transition dominates the luminescence spectra, followed by blue light of $\Delta J = 3$ transition and lastly, red emission from $\Delta J = 1$ transition. Intensity ratio of yellow [Y] ($\Delta J = 2$) to blue [B] ($\Delta J = 3$) emission lines reflects neighbouring environment experienced by Dy(III) ion in **Dy1–Dy4**.[54] In this study, the Y/B ratio is pointing towards a highly asymmetric surrounding in the solid phase.

3.5.4 Decay analysis and quantum yield. Fig. 6 depicts emission lifetime curves associated with **Dy1–Dy4** acquired by examining emission at 574 nm with excitation at about 370 nm. These curves were properly fitted by a single exponential function (eqn (3)),[55] yielding lifetime of τ (in ms) = 0.46, 0.65, 0.76 and 0.37 for **Dy1–Dy4**, respectively. This result strongly supports the existence of a single emissive center within the complexes.[56]

$$I = I_0 e^{(-t/\tau)} \quad (3)$$

The above relation expresses exponential decay of intensity I over time t, characterized by the decay time constant τ and initial intensity I_0. It is noteworthy to emphasize that upon coordinating three hfpd units (possessing low-energy C–F oscillators) alongside auxiliary ligands enables the emissive ions in these complexes to attain coordinative saturation. Additionally, these ligands shield the metal ion from external disturbances. Table 5 presents the data that was obtained through this analysis.

Photoluminescence quantum yield quantifies the proportion of absorbed photons that are re-emitted, typically in the visible spectrum, through the process of photoluminescence. To understand the effect of ancillary ligands on the

Table 5 Branching ratio of characteristic peaks for dysprosium and intensity ratio, lifetime and quantum yield across Dy1–Dy4

Complex	Branching ratio				Intensity ratio	Lifetime (ms)	Quantum yield (%)
	Ligand based band	$\Delta J = 3$	$\Delta J = 2$	$\Delta J = 1$			
Dy1	11.894	23.441	54.992	9.671	2.34	0.46	1.9
Dy2	15.703	11.605	68.556	4.134	5.90	0.65	2.7
Dy3	15.069	16.997	61.525	6.407	3.61	0.76	3.4
Dy4	90.616		7.987	1.395	—	0.37	1.2

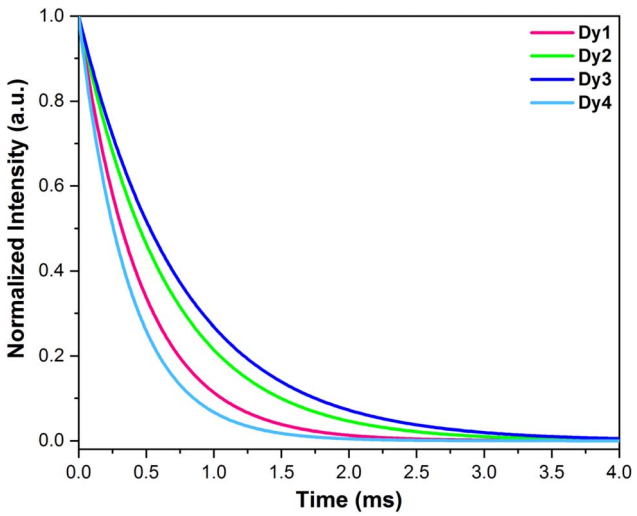

Fig. 6 Luminescence decay profiles of Dy1–Dy4 complexes.

photoluminescent characteristics, the luminescence quantum yields of the synthesized complexes were calculated using eqn (4) and are tabulated in Table 5. These calculations were carried out in DCM against quinine bisulphate in 1 M H_2SO_4 ($\Phi_r = 0.546$).[57,58]

$$\phi_S = \frac{\phi_r A_r I_S n_S^2}{A_r I_S n_r^2} \quad (4)$$

Here, Φ, A, I, n, r and s are quantum yield, absorbance at excitation wavelength, integrated emission intensity, refractive index, reference and sample, respectively.[59] Complex **Dy4** exhibited lowest quantum yield which could be attributed to back energy transfer whereas highest quantum yield amongst the synthesized samples was exhibited by **Dy3** suggesting better sensitizing nature of neoc unit.

3.5.5 Color parameters. Evaluation of emitted color and its quality from the solid Dy^{3+} complexes involved the use of CIE color coordinates and Correlated Color Temperature (CCT) values, as detailed in Table 6 and Fig. 7. The emission spectrum was employed to calculate x and y (CIE color coordinates), providing information on the color emitted by these ternary complexes. The conversion from x, y coordinates to 1976 CIE uniform chromaticity coordinates (u', v') (Fig. 8) was accomplished by employing eqn (5), utilizing the x, y values determined previously.[60,61]

$$u' = \frac{4x}{-2x + 12y + 3}, v' = \frac{9y}{-2x + 12y + 3} \quad (5)$$

CCT serves as a standard for assessing the properties of light imparted by a light source, playing a critical role in alleviating mental and visual stress. The careful selection of an appropriate CCT is crucial for ensuring effective lighting. Generally, a CCT value below 3200 K suggests warm white light, ideal for residential use, while a value exceeding 4000 K implies cold white light, often preferred for commercial lighting.[62,63] Calculation of these values was performed using McCamy's equation (eqn (6)):[64,65]

Table 6 Color Characteristics corresponding to Dy1 to Dy4

Complex	(x, y)	(u', v')	CCT
Dy1	(0.3191, 0.3143)	(0.2081, 0.4612)	6240.99
Dy2	(0.3330, 0.3305)	(0.2114, 0.4722)	5467.00
Dy3	(0.3545, 0.3714)	(0.2101, 0.4954)	4733.92
Dy4	(0.2206, 0.3086)	(0.1409, 0.4435)	>10 000

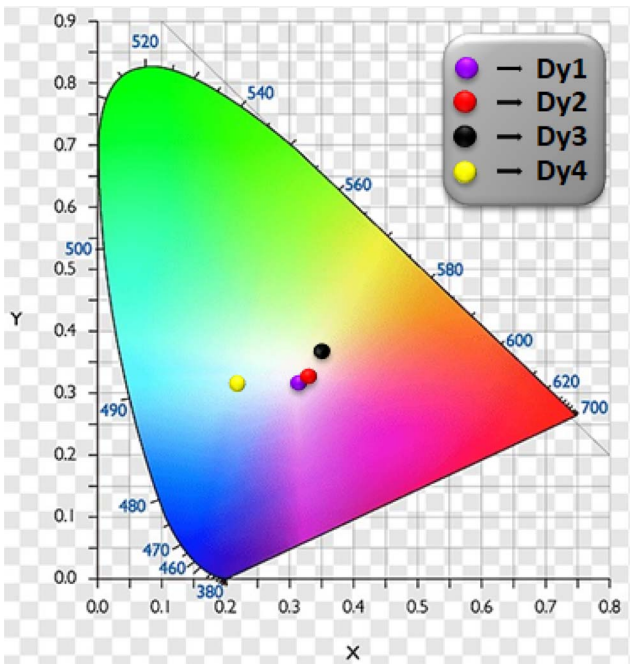

Fig. 7 CIE 1931 color coordinates of Dy1–Dy4 complexes.

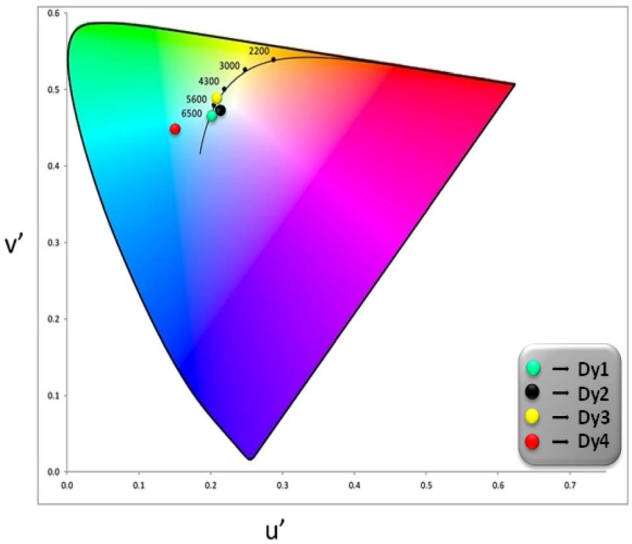

Fig. 8 CIE 1976 color coordinates for **Dy1–Dy4** complexes.

$$\mathrm{CCT} = -437n^3 + 3601n^2 - 6861n + 5514.31 \quad (6)$$

The variable n in the provided equation corresponds to the inverse slope of line and its calculation can be executed according to eqn (7).[66,67]

$$n = \frac{(x - x_e)}{(y - y_e)} \quad (7)$$

Here, x_e (0.332) and y_e (0.186) denote color epicentre. Complexes with ligands, TOPO, phen and neoc, are emitting in the region of cold white light at $\lambda_{ex} = 370$ nm. The CCT values recorded for these complexes are between 4733 to 6240 K, indicating the complexes' potential for applications in cold white light, particularly in commercial lighting. CIE data shows **Dy2** emits white light (CIE x, $y \approx 0.333$), with CCT around 5467.004 K. **Dy1** leans towards cold-white (bluish), while **Dy3** exhibits cold-white (yellowish) emission. However, subtle differences emerge for **Dy4** due to presence of a broad ligand based emission band in blue region. This color tunability is attained by modifying the coordination environment with various ancillary ligands.

3.5.6 Dependence of color coordinates on excitation wavelength. In an attempt to study the potential modulation of color in CIE graphs, the photoluminescence spectra of **Dy3** complex was recorded at various excitation wavelengths (250 nm to 380 nm). The resulting emission data was used to generate the emission map (Fig. 9). It was observed that the intensity of the emission spectra varies with the excitation wavelength, indicating that the emissive color coordinates are also influenced by the excitation wavelength. The emission data was analyzed to determine the x and y color coordinates (Table S1†) which were subsequently plotted on a CIE 1931 diagram for color visualization (Fig. 10). Utilizing eqn (4), the u', v' chromaticity coordinates were calculated and plotted on CIE 1976 color triangle (Fig. S6†). The dependence of color coordinates on excitation wavelength is shown in Fig. 10 & S6.† This

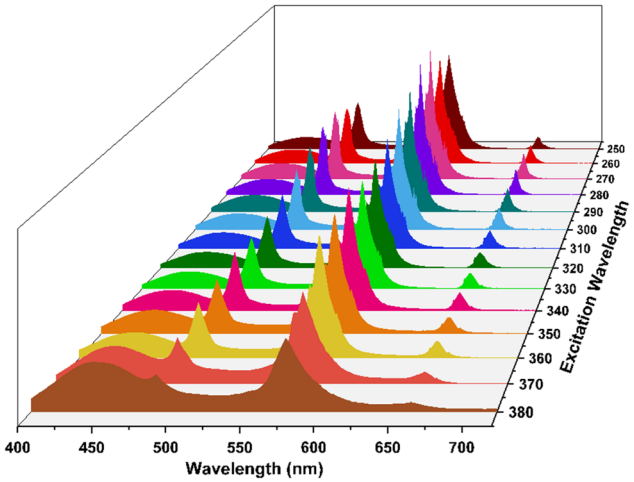

Fig. 9 Emission Map of **Dy3** at different excitation wavelengths.

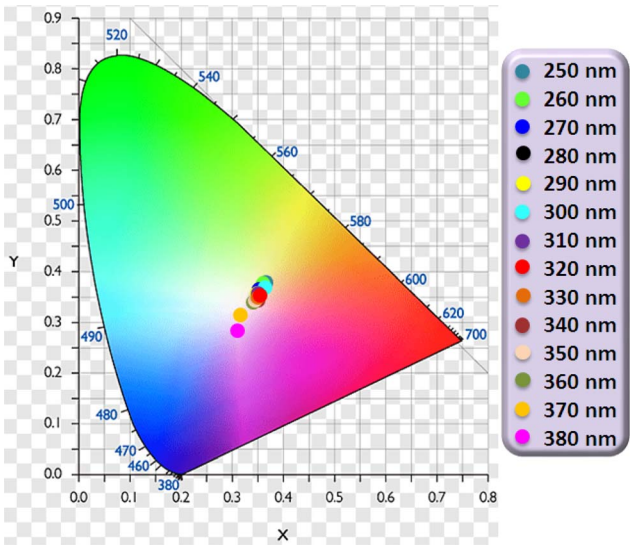

Fig. 10 CIE 1931 color coordinates for **Dy3** complex at different λ_{ex}.

comprehensive analysis provides insights into the tunability of emission properties and the potential for modulating the color output paving the way for future applications in color-tunable photonic devices.

3.5.7 Energy transfer mechanism. Understanding the photoluminescent behaviour of Dy(III) complexes requires careful examination of energy transfer pathways between dysprosium ion and coordinated ligands. Intramolecular energy transfer (IET) mechanism described by Dexter and Sato *et al.* states that two processes are mainly responsible for the IET efficiency.[68,69] (i) Through resonant exchange interaction, energy migrates from T_1 of organic ligand to emissive level of Ln^{3+} ion. (ii) Through a process known as thermal deactivation, energy is migrated inversely from Ln ion back to organic moiety. Back energy transfer (BET) predominates when the energy difference (ΔE) is too small for coordinated ligands and metal ion. ΔE plays a very significant role in energy transfer *via* above

mentioned processes. However inefficient ligand-to-metal sensitization due to BET can be overcome by vibrationally-assisted energy transfer.[70] This holds particular significance in Dy^{3+} coordination compounds, having main and long-lived emitting level, $^4F_{9/2}$, positioned at approximately 20 833 cm^{-1} which is relatively higher when compared to the T_1 of the majority of aromatic organic ligands. However, Dy(III) complexes lacks a reported optimal energy gap as suggested by Latva that would support efficient IET.[71]

The energy levels of the ligands (employed in complexation in **Dy1–Dy4**) in their triplet states are 21 978 cm^{-1} (TOPO),[72] 22 100 cm^{-1} (phen),[73] 22 624 cm^{-1} (neoc),[74] 20 163 cm^{-1} (bathoc)[75] and 21 930 cm^{-1} (hfpd).[76] The ΔE between emissive level of Dy(III) ion and T_1 of ligands is 1145 cm^{-1} (TOPO), 1267 cm^{-1} (phen), 1791 cm^{-1} (neoc), −670 cm^{-1} (bathoc) and 1097 cm^{-1} (hfpd). Energy transfer process in considered complexes is shown in Fig. 11. The relatively small ΔE is the contributing factor to BET from Dy^{3+} to organic ligands which is observed as a ligand based band in the emission spectrum of all the complexes. The most favourable ΔE has been observed for **Dy3** complex which results in least BET and most intense emission (Fig. S7 and S8†). While, least favourable ΔE is found for **Dy4** where the T_1 state of the ancillary ligand is positioned lower than the emissive state of the dysprosium ion, hindering efficient IET and promoting BET, resulting in a broad ligand based emission. Between **Dy1** and **Dy2** complex, better luminescence enhancement of Dy(III) ion is observed in **Dy2** owing to higher energy of T_1 state of phen in comparison to T_1 state of TOPO. Above that, the overall intensites of these complexes is low in comparison to the other reported compounds with europium, terbium and samarium metal ion, owing to less ΔE between emissive state of Dy and T_1 state of hfpd.[26]

3.6 CV analysis

For the purpose of studying electrochemical characteristics of synthesized **Dy1–Dy4** complexes, CV scans were recorded in DCM utilizing Fc/Fc^+ (ferrocene/ferricenium) redox couple ion as internal standard. A three-electrode system comprising of working electrode (glassy carbon), reference electrode (Ag/AgCl) and a counter electrode (Pt. wire) were employed along with supporting electrolyte (Tetra-*n*-butylammonium perchlorate) to obtain the CV curves (Fig. 12).

Utilizing data obtained from a CV plot, the oxidation (E_{ox}) and reduction (E_{red}) potentials were determined, resulting in values of 3.12 V (**Dy1**), 2.89 V (**Dy2**), 2.78 V (**Dy3**), 2.80 V (**Dy4**) for oxidation and −0.79 V (**Dy1**), −0.88 V (**Dy2**), −0.86 V (**Dy3**), −0.79 V (**Dy4**) for reduction. All the complexes exhibited a reversible electrochemical behaviour. Estimation of the energy of frontier molecular orbitals (FMO) involves the incorporation of the E_{ox} and E_{red} values into eqn (8) and (9).[77,78]

$$E_{HOMO} = -[(E_{ox} - E_{1/2(ferrocene)}) + 4.8]\ eV \quad (8)$$

$$E_{LUMO} = -[(E_{red} - E_{1/2(ferrocene)}) + 4.8]\ eV \quad (9)$$

The CV data of trivalent dysprosium complexes are tabulated in Table 7. $E_{1/2}$ of Fc as determined from their CV curve is equal to 1.03 V.[79] From values of FMOs, electronic band gap (E_g^b) of **Dy1–Dy4** complexes was calculated which exhibited a decreasing order by virtue of extended pi-electron conjugation. The electronic band gap values ranging from 3 to 4 eV confirm their semiconducting properties, making them suitable for application in display devices.

3.7 Thermal characterization

One of the key advantages of lanthanide complexes for use in optoelectronic devices is their remarkable thermal stability. This stability is clearly evident in Fig. 13, which shows the thermogravimetric (TG) plot over a wide range (25–650 °C). As the TG plot demonstrates, **Dy4** remains stable up to a temperature of 208 °C. However, at 210 °C and 578 °C, inflection point

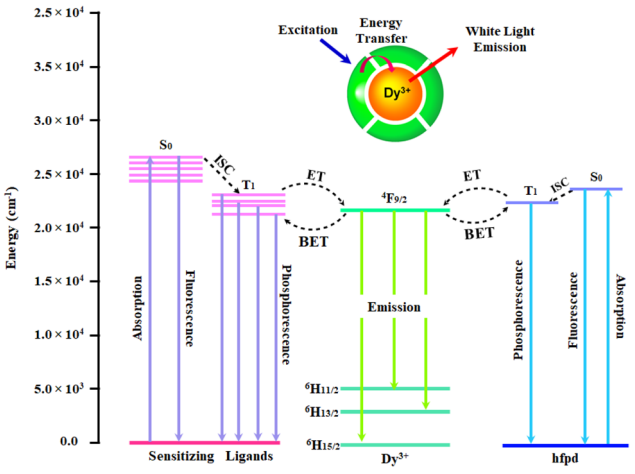

Fig. 11 Schematic diagram showing energy levels and energy transfer pathway in **Dy1–Dy4** (S_0: Singlet; T_1: Triplet; ISC: Inter System Crossing; ET: Energy Transfer; BET: Back Energy Transfer).

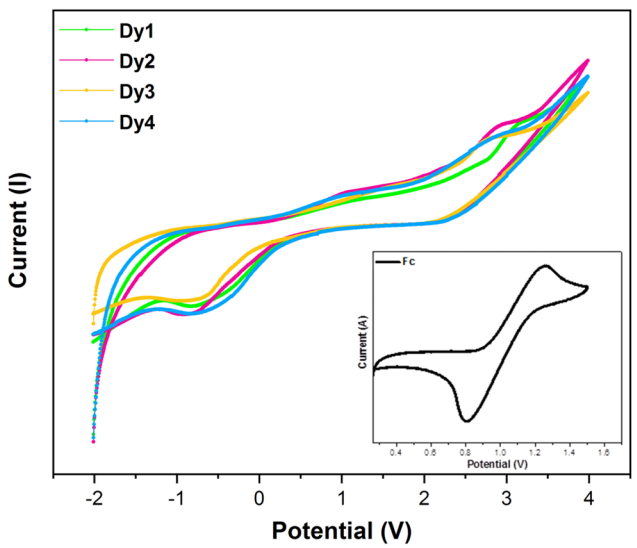

Fig. 12 CV profiles of **Dy1** and **Dy4**, with the inset displaying the CV profile of ferrocene.

Table 7 Comparative analysis of redox potential and electronic E_g^b for Dy1–Dy4

Complex	$^aE_{ox}$	$^aE_{red}$	$^aE_{HOMO}$	$^aE_{LUMO}$	$^aE_g^b$
Dy1	3.12	−0.79	−6.89	−2.98	3.91
Dy2	2.89	−0.88	−6.66	−2.89	3.77
Dy3	2.78	−0.86	−6.55	−2.91	3.64
Dy4	2.80	−0.79	−6.57	−2.98	3.59

^{a} E_{ox} and E_{red} are in (V); E_{HOMO}, E_{LUMO} and E_g^b are in (eV).

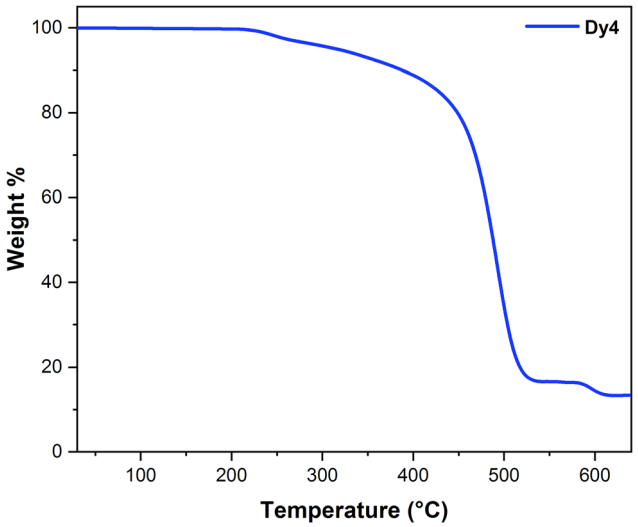

Fig. 13 Thermogravimetric curve of **Dy4** complex.

was observed on the TG plot, corresponding to 88.43% (calcd.: 86.06%) weight loss. This sharp change in weight indicates decomposition of **Dy4**. This remarkable stability makes it a promising candidate for various applications in optoelectronic devices. Above 617 °C, dysprosium oxide (Dy_2O_3) is identified as the stable oxide residue. The absence of an inflection point in the thermogram before 200 °C implies the absence of water, whether crystalliferous or coordinated.[80,81]

4 Conclusions

Heteroleptic ternary anhydrous dysprosium fluorinated β-diketonates were synthesized in one-step using four different auxiliary ligands of varying denticities. The triplet (T_1) states of ligands show close alignment with the emissive level of Dy^{3+} ion ($^4F_{9/2}$) which induced BET from this emissive state to the excited states of ligand. Consequently, this phenomenon gave rise to ligand based emission in blue region along with yellow-blue emission from Dy^{3+} ion. This characteristic was used to achieve near white-light emission. The observed white light emission (WLE) of **Dy1** ($x = 0.3191, y = 0.3143$), **Dy2** (0.3330, 0.3305) and **Dy3** (0.3545, 0.3714) is in close proximity to ideal white light, with CCT values in cold white-light region. From the study, it was found that the yellow emission in synthesized complexes is significantly influenced by the choice of coordinating moieties. Furthermore, the color coordinates are also influenced by the excitation wavelength used while recording the emission spectra. These complexes have applications in lasers, WLEDs, photoluminescent films and optoelectronic devices due to their semiconducting nature and large thermal stability. Additionally, the potential for wider utilization in multifunctional molecular materials, such as lighting and molecular magnets, introduces an intriguing element for further design exploration.

Data availability

The authors affirm that the information/data of this research article is available inside the article.

Author contributions

Sofia Malik = data curation, writing – original draft; Komal Jakhar and Devender Singh = writing – review & editing and supervision; Anjli Hooda = formal analysis; Sonia Redhu = methodology; Swati Dalal = data curation; Vandana Aggarwal = investigation; Sumit Kumar = visualization; Rajender Singh Malik = resources and validation; Parvin Kumar = project administration.

Conflicts of interest

The authors declare that they have no known competing financial interests or personal relationships that could have appeared to influence the work reported in this paper.

Acknowledgements

Sofia Malik is thankful to UGC-New Delhi for providing JRF [221610212505].

References

1 E. F. Schubert and J. K. Kim, Solid-state light sources getting smart, *Science*, 2005, **308**, 1274–1278, DOI: 10.1126/science.1108712.
2 P. Kumar, S. Singh, I. Gupta, K. Nehra, V. Kumar and D. Singh, Structural refinement and optical characteristics of single-phase $Gd_3Al_5O_{12}$: Er^{3+} nanophosphors for luminescent applications, *J. Lumin.*, 2022, **252**, 119338, DOI: 10.1016/j.jlumin.2022.119338.
3 I. Gupta, D. Singh, S. Singh, P. Kumar, S. Bhagwan and V. Kumar, Study of structural and spectroscopic characteristics of novel color tunable yellowish-white Dy^{3+} doped $Gd_4Al_2O_9$ nanophosphors for NUV-based WLEDs, *J. Mol. Struct.*, 2023, **1272**, 134199, DOI: 10.1016/j.molstruc.2022.134199.
4 I. Gupta, D. Singh, S. Singh, P. Kumar, S. Bhagwan and V. Kumar, Phase recognition and spectroscopic characteristics of single-phase Tb^{3+} doped $Gd_4Al_2O_9$ nanophosphors for NUV energized advanced photonic

appliances, *J. Lumin.*, 2022, **252**, 119327, DOI: 10.1016/j.jlumin.2022.119327.

5 A. De Almeida, B. Santos, B. Paolo and M. Quicheron, Solid state lighting review–Potential and challenges in Europe, *Renewable Sustainable Energy Rev.*, 2014, **34**, 30–48, DOI: 10.1016/j.rser.2014.02.029.

6 N. T. Kalyani and S. J. Dhoble, Organic light emitting diodes: Energy saving lighting technology—A review, *Renewable Sustainable Energy Rev.*, 2012, **16**, 2696–2723, DOI: 10.1016/j.rser.2012.02.021.

7 T. S. Mahapatra, H. Singh, A. Maity, A. Dey, S. K. Pramanik, E. Suresh and A. Das, White-light-emitting lanthanide and lanthanide-iridium doped supramolecular gels: modular luminescence and stimuli-responsive behaviour, *J. Mater. Chem. C*, 2018, **6**, 9756–9766, DOI: 10.1039/C8TC03487G.

8 V. Aggarwal, D. Singh, A. Hooda, S. Malik, S. Dalal, S. Redhu, S. Kumar, R. S. Malik and P. Kumar, Comprehensive investigation of ternary dysprosium complexes for white light emission: Synthesis, spectroscopic and colorimetric analyses, *J. Lumin.*, 2024, **270**, 120555, DOI: 10.1016/j.jlumin.2024.120555.

9 L. Xu, Y. Li, Q. Pan, D. Wang, S. Li, G. Wang, Y. Chen, P. Zhu and W. Qin, Dual-mode light-emitting lanthanide metal–organic frameworks with high water and thermal stability and their application in white LEDs, *ACS Appl. Mater. Interfaces*, 2020, **12**, 18934–18943, DOI: 10.1021/acsami.0c02999.

10 M. Chen, Y. Zhao, L. Yan, S. Yang, Y. Zhu, I. Murtaza, G. He, H. Meng and W. Huang, A Unique Blend of 2-Fluorenyl-2-anthracene and 2-Anthryl-2-anthracence Showing White Emission and High Charge Mobility, *Angew. Chem., Int. Ed.*, 2017, **56**, 722–727, DOI: 10.1002/anie.201608131.

11 Z. Xie, Q. Huang, T. Yu, L. Wang, Z. Mao, W. Li, Z. Yang, Y. Zhang, S. Liu, J. Xu, Z. Chi and M. P. Aldred, Hydrogen-Bonding-Assisted Intermolecular Charge Transfer: A New Strategy to Design Single-Component White-Light-Emitting Materials, *Adv. Funct. Mater.*, 2017, **27**, 1703918, DOI: 10.1002/adfm.201703918.

12 J. Manzur, R. C. De Santana, L. J. Q. Maia, A. Vega and E. Spodine, Tuning white light emission in dinuclear phenoxo bridged DyIII complexes, *Inorg. Chem.*, 2019, **58**, 10012–10018, DOI: 10.1021/acs.inorgchem.9b01153.

13 G. L. Law, K. L. Wong, H. L. Tam, K. W. Cheah and W. T. Wong, White OLED with a single-component europium complex, *Inorg. Chem.*, 2009, **48**, 10492–10494, DOI: 10.1021/ic9018037.

14 S. Redhu, D. Singh, A. Hooda, S. Malik, V. Aggarwal, S. Dalal, S. Kumar, R. S. Malik and P. Kumar, Synthesis, characterization and luminescent properties of N-donor based samarium-tris-β-diketonate: Tuning optoelectronic characteristics for displays applications, *J. Mol. Struct.*, 2024, **1308**, 138056, DOI: 10.1016/j.molstruc.2024.138056.

15 A. Dalal, K. Nehra, A. Hooda, S. Singh, S. Bhagwan, D. Singh and S. Kumar, 2, 2′-Bipyridine based fluorinated β-Diketonate Eu (III) complexes as red emitter for display applications, *Inorg. Chem. Commun.*, 2022, **140**, 109399, DOI: 10.1016/j.inoche.2022.109399.

16 P. P. F. da Rosa, Y. Kitagawa and Y. Hasegawa, Luminescent lanthanide complex with seven-coordination geometry, *Coord. Chem. Rev.*, 2020, **406**, 213153, DOI: 10.1016/j.ccr.2019.213153.

17 S. Redhu, D. Singh, A. Hooda, S. Malik, V. Aggarwal, S. Dalal, S. Kumar, R. S. Malik and P. Kumar, Photoluminescence tuning of terbium tris-1, 1, 1-trifluoro-5, 5-dimethyl-2, 4-hexanedione complexes: Synthesis, spectroscopic, thermal and electrochemical analyses, *J. Lumin.*, 2024, **271**, 120588, DOI: 10.1016/j.jlumin.2024.120588.

18 L. Zhong, W. B. Chen, Z. J. OuYang, M. Yang, Y. Q. Zhang, S. Gao, M. Schulze, W. Wernsdorfer and W. Dong, Unprecedented one-dimensional chain and two-dimensional network dysprosium (III) single-molecule toroics with white-light emission, *Chem. Commun.*, 2020, **56**, 2590–2593, DOI: 10.1039/C9CC08852K.

19 L. Zhong, W. B. Chen, X. H. Li, Z. J. OuYang, M. Yang, Y. Q. Zhang, S. Gao and W. Dong, Four dinuclear and one-dimensional-chain dysprosium and terbium complexes based on 2-Hydroxy-3-methoxybenzoic acid: Structures, fluorescence, single-molecule-magnet, and ab initio investigation, *Inorg. Chem.*, 2020, **59**, 4414–4423, DOI: 10.1021/acs.inorgchem.9b03555.

20 D. Mara, L. Pilia, M. Van de Steen, I. Miletto, M. Zeng, K. Van Hecke, A. Serpe, P. Deplano, R. Van Deun and F. Artizzu, Single-component panchromatic white light generation, and tuneable excimer-like visible orange and NIR emission in a Dy quinolinolate complex, *J. Mater. Chem. C*, 2021, **9**, 15641–15648, DOI: 10.1039/D1TC04191F.

21 S. Redhu, D. Singh, K. Nehra, S. Dalal, S. Malik, V. Aggarwal, S. Kumar, R. S. Malik, P. Kumar and J. Sindhu, NUV-excitation Dy (III) complexes: Synthesis, structural study and impact of secondary ligands on optoelectronic properties, *J. Mol. Struct.*, 2024, **1311**, 138380, DOI: 10.1016/j.molstruc.2024.138380.

22 A. Hooda, K. Nehra, A. Dalal, S. Singh, R. K. Saini, S. Kumar and D. Singh, Terbium complexes of an asymmetric β-diketone: preparation, photophysical and thermal investigation, *Inorg. Chim. Acta*, 2022, **536**, 120881, DOI: 10.1016/j.ica.2022.120881.

23 R. F. Li, R. H. Li, X. F. Liu, X. H. Chang and X. Feng, Lanthanide complexes based on a conjugated pyridine carboxylate ligand: structures, luminescence and magnetic properties, *RSC Adv.*, 2020, **10**, 6192–6199, DOI: 10.1039/C9RA10975G.

24 K. Nehra, A. Dalal, A. Hooda, S. Bhagwan, R. K. Saini, B. Mari, S. Kumar and D. Singh, Lanthanides β-diketonate complexes as energy-efficient emissive materials: A review, *J. Mol. Struct.*, 2022, **1249**, 131531, DOI: 10.1016/j.molstruc.2021.131531.

25 S. Ahmad Bhat and K. Iftikhar, Optical Properties of New Terbium (III) Ternary Complexes Containing Anionic 6, 6, 7, 7, 8, 8, 8-heptafluoro-2, 2-dimethyl-3, 5-octanedione and Neutral Sensitizers in Solution, Solid and PMMA Thin Films: Intra and Interphase Colour Tuning, *J. Photochem. Photobiol.*, 2021, **97**, 688–699, DOI: 10.1111/php.13382.

26 Z. Ahmed and K. Iftikhar, Synthesis, luminescence and NMR studies of lanthanide (III) complexes with hexafluoroacetylacetone and phenanthroline. Part II, *Inorg. Chim. Acta*, 2012, **392**, 165–176, DOI: 10.1016/j.ica.2012.06.032.

27 J. Rocha, C. D. Brites and L. D. Carlos, Lanthanide organic framework luminescent thermometers, *Chem. - Eur. J.*, 2016, **22**, 14782–14795, DOI: 10.1002/chem.201600860.9756.

28 A. Dalal, K. Nehra, A. Hooda, S. Singh, S. Bhagwan, D. Singh and S. Kumar, 2, 2′-Bipyridine based fluorinated β-Diketonate Eu (III) complexes as red emitter for display applications, *Inorg. Chem. Commun.*, 2022, **140**, 109399, DOI: 10.1016/j.inoche.2022.109399.

29 D. Mara, F. Artizzu, B. Laforce, L. Vincze, K. Van Hecke, R. Van Deun and A. M. Kaczmarek, Novel tetrakis lanthanide β-diketonate complexes: Structural study, luminescence properties and temperature sensing, *J. Lumin.*, 2019, **213**, 343–355, DOI: 10.1016/j.jlumin.2019.05.035.

30 L. Ruan, X. Gao, J. Zhao, C. Xu and D. Liang, Preparation and characteristics of Eu(DBM)$_3$phen: Synthesis, single-crystal structure and spectroscopic analysis, *J. Mol. Struct.*, 2017, **1149**, 265–272, DOI: 10.1016/j.molstruc.2017.08.003.

31 A. Hooda, D. Singh, K. Nehra, S. Dalal, V. Aggarwal, S. Kumar, R. S. Malik and P. Kumar, Preparation and optical studies of octacoordinated luminescent complexes of Dy(III) derived from fluorinated β-diketone and heteroaromatic neutral ligands, *Inorg. Chim. Acta*, 2023, **556**, 121674, DOI: 10.1016/j.ica.2023.121674.

32 H. Ogoshi and K. Nakamoto, Normal-Coordinate Analyses of Hydrogen-Bonded Compounds. V. The Enol Forms of Acetylacetone and Hexafluoroacetylacetone, *J. Chem. Phys.*, 1966, **45**, 3113–3120, DOI: 10.1063/1.1728068.

33 S. Dasari, S. Singh, P. Kumar, S. Sivakumar and A. K. Patra, Near-infrared excited cooperative upconversion in luminescent Ytterbium (III) bioprobes as light-responsive theranostic agents, *Eur. J. Med. Chem.*, 2019, **163**, 546–559, DOI: 10.1016/j.ejmech.2018.12.010.

34 M. Sengar and A. K. Narula, Luminescence sensitization of Eu (III) complexes with aromatic Schiff base and N, N'-donor heterocyclic ligands: synthesis, luminescent properties and energy transfer, *J. Fluoresc.*, 2019, **29**, 111–120, DOI: 10.1007/s10895-018-2315-3.

35 S. Malik, K. Jakhar, D. Singh, S. Dalal, A. Hooda, K. Nehra, S. Kumar, R. S. Malik and P. Kumar, Exploring the role of neutral ligands in modulating the photoluminescence of samarium complexes with 1, 1, 1, 5, 5, 5-hexafluoro-2, 4-pentanedione, *Luminescence*, 2024, **39**, e4810, DOI: 10.1002/bio.4810.

36 L. Li, J. Gou, D. F. Wu, Y. J. Wang, Y. Y. Duan, H. H. Chen, H. L. Gao and J. Z. Cui, Near-infrared luminescence and magnetic properties of dinuclear rare earth complexes modulated by β-diketone co-ligands, *New J. Chem.*, 2020, **44**, 3912–3921, DOI: 10.1039/D0NJ00164C.

37 R. Ilmi and K. Iftikhar, Optical emission studies of new europium and terbium dinuclear complexes with trifluoroacetylacetone and bridging bipyrimidine. Fast radiation and high emission quantum yield, *Polyhedron*, 2015, **102**, 16–26, DOI: 10.1016/j.poly.2015.07.046.

38 A. Hooda, A. Dalal, K. Nehra, D. Singh, S. Kumar, R. S. Malik and P. Kumar, Preparation and optical investigation of green luminescent ternary terbium complexes with aromatic β-diketone, *Chem. Phys. Lett.*, 2022, **794**, 139495, DOI: 10.1016/j.cplett.2022.139495.

39 Z. Ahmed and K. Iftikhar, Sensitization of visible and NIR emitting lanthanide (III) ions in noncentrosymmetric complexes of hexafluoroacetylacetone and unsubstituted monodentate pyrazole, *J. Phys. Chem. A*, 2013, **117**, 11183–11201, DOI: 10.1021/jp403668j.

40 Y. Y. Duan, D. F. Wu, H. H. Chen, Y. J. Wang, L. Li, H. L. Gao and J. Z. Cui, New dinuclear lanthanide complexes derived from Schiff base ligand and β-diketonate co-ligand: Synthesis, crystal structures, luminescent and magnetic properties, *Polyhedron*, 2022, **225**, 116070, DOI: 10.1016/j.poly.2022.116070.

41 R. Ilmi and K. Iftikhar, Synthesis and photoluminescence properties of pink luminescent heteroleptic Sm(III) complexes; the role of DMSO in transforming the inner coordination sphere and on photophysical properties. Sparkle/RM1 calculation, *Polyhedron*, 2017, **127**, 191–202, DOI: 10.1016/j.poly.2017.01.035.

42 Z. Ahmed and K. Iftikhar, Efficient photoluminescent complexes of 400–1800 nm wavelength emitting lanthanides containing organic sensitizers for optoelectronic devices, *RSC Adv.*, 2014, **4**, 63696–63711, DOI: 10.1039/C4RA11330F.

43 D. Singh, K. Nehra, R. K. Saini, A. Dalal, S. Bhagwan, K. Singh, A. P. Simantilleke and S. Kumar, Luminescence intensification of terbium(III) ion complexes with dipivaloylmethane (tmhd) and monodentate auxiliary ligands, *Optik*, 2020, **206**, 164338, DOI: 10.1016/j.ijleo.2020.164338.

44 S. Dalal, D. Singh, A. Dalal, A. Hooda, S. Malik, S. Kumar, R. S. Malik, P. Kumar and J. Sindhu, Samarium (III) complexes with tunable luminescence: efficient sensitization and semiconducting properties for optoelectronic devices, *J. Mater. Sci.: Mater. Electron.*, 2024, **35**, 632, DOI: 10.1007/s10854-024-12353-6.

45 A. Dalal, K. Nehra, A. Hooda, P. Kumar, D. Singh, S. Kumar, R. Kumar and P. Kumar, Red emissive β-diketonate Ln (III) complexes for displays: Preparation, spectroscopic and optical investigations, *Optik*, 2023, **276**, 170648, DOI: 10.1016/j.ijleo.2023.170648.

46 H. L. Wang, X. F. Ma, H. H. Zou, K. Wang, B. Li, Z. L. Chen and F. P. Liang, Mixed chelating ligands used to regulate the luminescence of Ln (III) complexes and single-ion magnet behavior in Dy-based analogues, *Dalton Trans.*, 2018, **47**, 15929–15940, DOI: 10.1039/C8DT03133A.

47 W. A. Dar, Z. Ahmed and K. Iftikhar, Cool white light emission from the yellow and blue emission bands of the Dy (III) complex under UV-excitation, *J. Photochem. Photobiol., A*, 2018, **356**, 502–511, DOI: 10.1016/j.jphotochem.2017.12.017.

48 A. Hooda, D. Singh, A. Dalal, S. Malik, S. Redhu, K. Jakhar, S. Kumar, R. S. Malik and P. Kumar, Preparation and spectral features of Dy(III) β-Diketonates with m,m′-Disubstituted N-donor aromatic auxiliary moieties for displays, *Inorg. Chem. Commun.*, 2023, **155**, 111018, DOI: 10.1016/j.inoche.2023.111018.

49 I. Gupta, S. Singh, P. Kumar, S. Bhagwan, V. Kumar and D. Singh, Structural, morphological and optoelectronic aspects of $YAlO_3$: Dy^{3+} doped nanocrystalline materials for NUV energized WLEDs, *Curr. Appl. Phys.*, 2022, **43**, 78–89, DOI: 10.1016/j.cap.2022.08.011.

50 F. Gu, S. F. Wang, M. K. Lü, G. J. Zhou, D. Xu and D. R. Yuan, Structure evaluation and highly enhanced luminescence of Dy^{3+}-doped ZnO nanocrystals by Li^{+} doping via combustion method, *Langmuir*, 2004, **20**, 3528–3531, DOI: 10.1021/la049874f.

51 S. Dalal, D. Singh, A. Hooda, S. Redhu, S. Malik, V. Aggarwal, S. Kumar, R. S. Malik, P. Kumar and J. Sindhu, Enhancement in photophysical properties of octacoordinated Dy (III) complexes via energy transfer from photosensitizing ligands, *Opt. Mater.*, 2024, **150**, 115159, DOI: 10.1016/j.optmat.2024.115159.

52 W. A. Dar, A. B. Ganaie and K. Iftikhar, Synthesis and photoluminescence study of two new complexes $[Sm(hfaa)_3(impy)_2]$ and $[Eu(hfaa)_3(impy)_2]$ and their PMMA based hybrid films, *J. Lumin.*, 2018, **202**, 438–449, DOI: 10.1016/j.jlumin.2018.05.032.

53 A. Pereira, G. Conte, A. D. Faceto, L. A. Nunes, W. G. Quirino, C. Legnani, H. Gallardo, M. Cremona, I. H. Bechtold and F. E. Guimarães, Influence of nonradiative Auger process in the lanthanide complexes lifetime near interfaces in organic light-emitting diode structures, *J. Appl. Phys.*, 2019, **126**, 165501, DOI: 10.1063/1.5099014.

54 A. Hooda, A. Dalal, K. Nehra, S. Singh, S. Kumar and D. Singh, Red-emitting β-diketonate Eu(III) Complexes With Substituted 1,10-phenanthroline Derivatives: Optoelectronic and Spectroscopic Analysis, *J. Fluoresc.*, 2022, **32**, 1413–1424, DOI: 10.1007/s10895-022-02951-0.

55 H. F. Li, P. F. Yan, P. Chen, Y. Wang, H. Xu and G. M. Li, Highly luminescent bis-diketone lanthanide complexes with triple-stranded dinuclear structure, *Dalton Trans.*, 2012, **41**, 900–907, DOI: 10.1039/C1DT11496D.

56 S. Malik, K. Jakhar, D. Singh, A. Hooda, K. Nehra, S. Kumar, R. S. Malik and P. Kumar, Near ultra-violet excitable Tb (III)-tris-hexafluoro-2, 4-pentanedione complexes for OLEDs: Insights into the impact of ancillary ligands on photoluminescent characteristics, *J. Mol. Struct.*, 2024, **1311**, 138334, DOI: 10.1016/j.molstruc.2024.138334.

57 K. Nehra, A. Dalal, A. Hooda, K. Jakhar, D. Singh and S. Kumar, Preparation, optoelectronic and spectroscopic analysis of fluorinated heteroleptic samarium complexes for display applications, *Inorg. Chim. Acta*, 2022, **537**, 120958, DOI: 10.1016/j.ica.2022.120958.

58 K. Nehra, A. Dalal, A. Hooda, S. Singh, D. Singh and S. Kumar, Spectroscopic and optical investigation of 1, 10-phenanthroline based Tb (III) β-diketonate complexes, *Inorg. Chim. Acta*, 2022, **536**, 120860, DOI: 10.1016/j.ica.2022.120860.

59 A. Dalal, K. Nehra, A. Hooda, D. Singh, K. Jakhar and S. Kumar, Preparation and photoluminescent characteristics of green Tb (III) complexes with β-diketones and N donor auxiliary ligands, *Inorg. Chem. Commun.*, 2022, **139**, 109349, DOI: 10.1016/j.inoche.2022.109349.

60 S. Singh, A. P. Simantilleke and D. Singh, Crystal structure and photoluminescence investigations of $Y_3Al_5O_{12}$:Dy^{3+} nanocrystalline phosphors for WLEDs, *Chem. Phys. Lett.*, 2021, **765**, 138300, DOI: 10.1016/j.cplett.2020.138300.

61 A. Dalal, A. Hooda, K. Nehra, D. Singh, S. Kumar, R. S. Malik and P. Kumar, Effect of substituted 2,2' -bipyridine derivatives on luminescence characteristics of green emissive terbium complexes: Spectroscopic and optical analysis, *J. Mol. Struct.*, 2022, **1265**, 133343, DOI: 10.1016/j.molstruc.2022.133343.

62 O. E. Zheleznikova, S. V. Prytkov and A. M. Kokinov, Selection of optimal method of correlated colour temperature calculation, *J. Mech. Contin. Math. Sci.*, 2020, **8**, 134–143, DOI: 10.26782/jmcms.spl.8/2020.04.00010.

63 I. Gupta, S. Singh, P. Kumar, S. Bhagwan, V. Kumar and D. Singh, Structural, morphological and optoelectronic aspects of $YAlO_3$: Dy^{3+} doped nanocrystalline materials for NUV energized WLEDs, *Curr. Appl. Phys.*, 2022, **43**, 78–89, DOI: 10.1016/j.cap.2022.08.011.

64 C. S. McCamy, Correlated color temperature as an explicit function of chromaticity coordinates, *Color Res. Appl.*, 1992, **17**, 142–144, DOI: 10.1002/col.5080170211.

65 P. Kumar, S. Singh, I. Gupta, A. Hooda, V. Kumar and D. Singh, Reddish-orange color tunable Sm^{3+} activated $Gd_3Al_5O_{12}$ phosphors: Crystallographic and photophysical investigation for lighting applications, *J. Mol. Struct.*, 2023, **1271**, 134074, DOI: 10.1016/j.molstruc.2022.134074.

66 K. Nehra, A. Dalal, A. Hooda, R. K. Saini, D. Singh and S. Kumar, Synthesis and photoluminescence characterization of the complexes of samarium dibenzoylmethanates with 1,10-phenanthroline derivatives, *Polyhedron*, 2022, **217**, 115730, DOI: 10.1016/j.poly.2022.115730.

67 A. Hooda, K. Nehra, A. Dalal, S. Singh, R. K. Saini, S. Kumar and D. Singh, Deep red emissive octacoordinated heteroleptic Sm (III) complexes: preparation and spectroscopic investigation, *J. Mol. Struct.*, 2022, **1260**, 132848, DOI: 10.1016/j.molstruc.2022.132848.

68 D. L. Dexter, A theory of sensitized luminescence in solids, *J. Chem. Phys.*, 1953, **21**, 836–850, DOI: 10.1063/1.1699044.

69 S. Sato and M. Wada, Relations between intramolecular energy transfer efficiencies and triplet state energies in rare earth β-diketone chelates, *Bull. Chem. Soc. Jpn.*, 1970, **43**, 1955–1962, DOI: 10.1246/bcsj.43.1955.

70 Y. Hasegawa and Y. Kitagawa, Luminescent lanthanide coordination polymers with transformative energy transfer processes for physical and chemical sensing applications, *J. Photochem. Photobiol., C*, 2022, **51**, 100485, DOI: 10.1016/j.jphotochemrev.2022.100485.

71 C. Doffek, J. Wahsner, E. Kreidt and M. Seitz, Breakdown of the energy gap law in molecular lanthanoid luminescence: the smallest energy gap is not universally relevant for nonradiative deactivation, *Inorg. Chem.*, 2014, **53**, 3263–3265, DOI: **10.1021/ic500017a**.

72 O. V. Kotova, S. V. Eliseeva, A. A. Volosnikov, V. A. Oleinikov, L. S. Lepnev, A. G. Vitukhnovskii and N. P. Kuz'mina, Influence of heteroligand complexation on the thermal, photoluminescent, and film-forming properties of some aromatic terbium (III) carboxylates, *Russ. J. Coord. Chem.*, 2006, **32**, 901–909, DOI: **10.1134/S1070328406120086**.

73 H. Yu, Q. Liu, J. Li, Z. M. Su, X. Li, X. Wang, X. Wang, J. Sun, C. Zhou and X. Hu, A dual-emitting mixed-lanthanide MOF with high water-stability for ratiometric fluorescence sensing of Fe^{3+} and ascorbic acid, *J. Mater. Chem. C*, 2021, **9**, 562–568, DOI: **10.1039/D0TC04781C**.

74 S. Malik, K. Jakhar, D. Singh, S. Kumar, R. S. Malik and P. Kumar, Optimizing hexafluoro-2, 4-pentanedione based Eu (III) complexes: A comprehensive study on the synthesis, spectroscopic characterization with Judd-Ofelt calculation, *Opt. Mater.*, 2024, **150**, 115257, DOI: **10.1016/j.optmat.2024.115257**.

75 V. I. Adamovich, S. R. Cordero, P. I. Djurovich, A. Tamayo, M. E. Thompson, B. W. D'Andrade and S. R. Forrest, New charge-carrier blocking materials for high efficiency OLEDs, *Org. Electron.*, 2003, **4**, 77–87, DOI: **10.1016/j.orgel.2003.08.003**.

76 R. Ilmi, D. Zhang, L. Tensi, H. Al-Sharji, N. K. Al Rasbi, A. Macchioni, L. Zhou, W. Y. Wong, P. R. Raithby and M. S. Khan, Salts of Lanthanide(III) Hexafluoroacetylacetonates [Ln= Sm(III), Eu(III) and Tb(III)] with Dipyridylammonium cations: Synthesis, characterization, photophysical properties and OLED fabrication, *Dyes Pigm.*, 2022, **203**, 110300, DOI: **10.1016/j.dyepig.2022.110300**.

77 A. Dalal, K. Nehra, A. Hooda, D. Singh, J. Dhankhar and S. Kumar, Fluorinated β-diketone-based Sm(III) complexes: spectroscopic and optoelectronic characteristics, *Luminescence*, 2022, **37**, 1328, DOI: **10.1002/bio.4300**.

78 A. Hooda, A. Dalal, K. Nehra, P. Kumar, D. Singh, S. Kumar, R. S. Malik, R. Kumar and P. Kumar, Mononuclear luminous β-diketonate Ln(III) complexes with heteroaromatic auxiliary ligands: synthesis and luminescence characteristics, *Luminescence*, 2022, **37**, 1921–1931, DOI: **10.1002/bio.4376**.

79 K. Nehra, A. Dalal, A. Hooda, D. Singh, R. S. Malik and S. Kumar, Spectroscopic and optoelectronic investigations of 3,8-Bis(3,4-(ethylenedioxy)thien-2-yl)-1,10-phenanthroline, *J. Mater. Sci.: Mater. Electron.*, 2022, **33**, 115–125, DOI: **10.1007/s10854-021-07268-5**.

80 M. I. Saleh, M. Y. Choo, T. W. Chan and M. R. Razali, Effect of second ligand on the luminescence of Samarium (III) dibenzoylmethane complexes: Syntheses, crystal structures, thermal analysis and luminescence study, *J. Chem. Sci.*, 2015, **127**, 2241–2249, DOI: **10.1007/s12039-015-0986-8**.

81 A. Hooda, K. Nehra, A. Dalal, S. Singh, S. Bhagwan, K. Jakhar and D. Singh, Preparation and photoluminescent analysis of Sm^{3+} complexes based on unsymmetrical conjugated chromophoric ligand, *J. Mater. Sci.: Mater. Electron.*, 2022, **33**, 11132–11142, DOI: **10.1007/s10854-022-08089-w**.